Highly permeable and highly selective ultrathin film composite polyamide membranes reinforced by reactable polymer chains

Zhikan Yao[a], Zhe Yang[a], Hao Guo[a], Xiaohua Ma[a,b], Yingchao Dong[c], and Chuyang Y. Tang[a*]

a. Department of Civil Engineering, The University of Hong Kong, Pokfulam, Hong Kong SAR.

b. Shanghai Key Laboratory of Multiphase Materials Chemical Engineering, Chemical Engineering Research Center, East China University of Science and Technology, 130 Meilong Road, Shanghai, China

c. Key Laboratory of Industrial Ecology and Environmental Engineering (MOE), School of Environmental Science and Technology, Dalian University of Technology, Dalian, China

*Corresponding author.

E-mail address: tangc@hku.hk (C.Y. Tang)

Abstract

This study reports highly permeable ultrathin film composite (uTFC) membranes whose rejection layer was reinforced by polymer chains during the interfacial polymerization of trimesoyl chloride (TMC) and m-phenylenediamine (MPD) to achieve enhanced salt rejection. A rejection layer of approximately 20 nm was formed at an MPD concentration of 0.01 wt%. This reinforced membrane had a water permeability of about 16.7 L/(m^2 h bar), while exhibiting an improved divalent salt (Na_2SO_4) to monovalent salt (NaCl) selectivity compared with the control TFC membrane without reinforcement (3.44 vs. 1.06). The role of the reactable polymer chains in interfacial polymerization was discussed as MPD adsorbent and reactant, according to the measurements by quartz crystal microbalance and X-ray photoelectron spectroscopy. This work provides a new pathway for the design and construction of uniform ultrathin layers as well as the preparation of high performance separation membranes.

Key words: thin film composite membrane, ultrathin rejection layer, interfacial polymerization, divalent to monovalent salts selectivity, reactable substrate

1. Introduction

Reverse osmosis (RO) and nanofiltration (NF) membranes are widely applied in desalination, wastewater reclamation, and water softening [1-4]. These membranes are typically composed of a thin polyamide rejection layer on top of a porous substrate (usually an ultrafiltration membrane). The polyamide rejection layer, formed by an interfacial polymerization reaction, largely determines the membrane separation properties [5-9]. Despite the great advancements achieved in the past decades, membranes with high permeability and high selectivity remain as a high priority research area [10-12].

One effective way to achieve high water permeability is to make an ultrathin rejection layer [13-16]. In principle, ultrathin film composite (uTFC) membranes can be prepared by reducing the concentrations of monomers used in the interfacial polymerization process (e.g., trimesoyl chloride (TMC) or m-phenylenediamine (MPD)) [17]. However, this approach often results in relatively low salt rejection due to its high propensity for defects formation [17, 18]. Some recent works report the use of an interlayer (e.g., cadmium hydroxide nanostrands [17], single-walled carbon nanotube (SWCNTs) [15], ZIF-8 [19] or tannic acid/Fe^{3+} complexes [20]) to minimize defects in the ultrathin rejection layer. Alternatively, molecular layer-by-layer deposition or stepwise interfacial polymerization [21, 22] can be employed. Unfortunately, the preparation process involves multiple steps of repeated coating,

which make the method difficult to scale up.

In our recent work [23], we reported the use of a reactable substrate to prepare polyamide rejection layers with enhanced crosslinking degree. Here, we extend this approach for the first time to the preparation of uTFC polyamide membranes. In viewing the ultrathin nature of their rejection layers, the separation performance of uTFC membranes is expected to have greater dependence on the substrate, whose role needs to be systematically investigated.

In the current study, uTFC membranes were prepared by a one-step interfacial polymerization on a substrate containing linear polymer chains that are designed to participate in the reaction and thus to reinforce the rejection layer. Separation performance tests showed greatly improved rejection of the polymer chain-reinforced uTFC membranes, revealing the critical importance of substrate design on the integrity of membranes with ultrathin rejection layers. The results in this study offer new views on the preparation of high performance uTFC membranes.

2. Experimental

2.1. Materials

Poly (vinyl chloride) (PVC, Mn ~ 47,000, Sigma-Aldrich), lithium chloride (LiCl, anhydrous, 99%, Sigma-Aldrich), N,N-dimethylacetamide (DMAc, 99%,

Sigma-Aldrich), polyethylene glycol (PEG, Mn ~ 400, AR, Dieckmann Company) and methyl methacrylate and 2-hydroxyethyl methacrylate copolymer (PMcH, Mn~37,200, HEMA content ~54.9%, synthesized following a previous procedure [23]) were used for the preparation of substrates. 1,3,5-benzenetricarbonyl trichloride (TMC, trimesoyl chloride, 98%, Sigma-Aldrich), n-hexane (for HPLC, ≥95%, Sigma-Aldrich), m-phenylenediamine (MPD, 99%, Sigma-Aldrich) and trisodium phosphate dodecahydrate ($Na_3PO_4 \cdot 12H_2O$, AR, Dieckmann company, used as the acid acceptor) were used for the preparation of the rejection layers. Analytical Reagent Sodium chloride (NaCl) and sodium sulfate (Na_2SO_4) were obtained from Dieckmann Company.

2.2. uTFC membrane synthesis

uTFC membranes in this study were prepared through the interfacial polymerization method on PVC-based substrates. Compared to commonly used polysulfone and polyethersulfone, PVC is a much cheaper material with broad commercial prospect in ultrafiltration membrane preparation. In addition, PVC-based substrates can be easily modified by blending poly(methyl methacrylate) based amphiphilic copolymers. In this study, pure PVC substrates (PVC-0) and reactable polymer chains contained substrates (PVC-r) were prepared following the reported method and used as substrates [23]. The interfacial polymerization process was as follow. The substrate was immersed in a MPD solution (0.01 wt% ~ 0.1 wt%, and additionally 0.6 wt%

Na_3PO_4) for 1 min. Then the excess MPD solution was removed by rolling a rubber roller. Afterward, the soaked substrate was immersed in a 0.05 wt% TMC-n-hexane solution for 30 seconds. The resultant membrane was rinsed with n-hexane to remove excess TMC solution and stored in a deionized water bath at 50 ℃ for 10 min. Finally, the obtained uTFC membrane was stored in deionized water until use. The uTFC membranes were named as uTFC-0-n or uTFC-r-n, where n referred to the MPD concentration in wt%. For example, uTFC-0-0.01 presents the uTFC membrane prepared by using PVC-0 as substrate and MPD solution with the concentration of 0.01 wt%.

2.3. Membrane characterization

Membrane structure and morphology were characterized by field-emission scanning electron microscopy (FE-SEM, S-4800, Hitachi) and transmission electron microscopy (TEM, CM100, Philips). To measure the rejection layer thickness, cross-section images obtained from SEM or TEM were analyzed using Image-Pro Plus software provided by Media Cybernetics, Inc. The membrane surface chemical composition was determined by the X-ray photoelectron spectroscopy (XPS, PHI 5000C ESCA system, PHI CO.). The X-ray source (Al K áradiation, 1486.6 eV) was run at a power of 250W (14.0 kV, 93.9 eV). The special electron incidence angle was 30 °, 60 ° or 90 °. The software AugerScan 3.2 (RBD Enterprises, Inc.) was employed to analyze the collected data. The surface charge properties of the membranes were

evaluated by SurPASS electrokinetic analyzer (SurPASS^{TM} 3, Anton Paar) following a standard operation [24].

2.4. Filtration tests

The filtration performances of the prepared uTFC membranes were evaluated by using a laboratory-scale cross-flow membrane filtration setup at around 25 ℃ [23]. A membrane sample was first pre-compacted at an applied pressure of 3.5 bar for about 2 h with feed solution (deionized water, 5 mmol/L Na_2SO_4 or 7.5 mmol/L NaCl) and then tested at 3 bar. Pure water flux of the membrane sample was measured by weighing the collected permeate water in several minutes. The salt rejection of the membrane sample was calculated according to the salt concentration in the permeate and the feed. The Na_2SO_4 to NaCl selectivity (α) was calculated by Eq. (1):

$$\alpha(NaCl/Na_2SO_4) = \frac{1-R_{NaCl}}{1-R_{Na2SO4}} \times 100\% \quad (1)$$

2.5. MPD adsorption experiment

Quartz crystal microbalance (QCM, QCM E4, Biolin Scientitic) was used to evaluate the MPD adsorption capacity of PVC and PMcH. A thin PVC or PMcH layer was coated on an Au-coated resonator by 0.05 wt% PVC-DMF solution or PMcH-DMF solution, respectively. The prepared resonator was set up in a fluid cell with the coated side exposed to the testing solution. The measurement of MPD adsorption was initiated by switching the liquid exposed to the resonator. MPD solution (with the

concentration of 0.1 wt% or 0.01 wt%) was allowed to contact with the resonator for about 30 min. Then, deionized water was introduced for about 10 min to wash out nonspecific adsorption MPD. The MPD adsorption data were analyzed according to the Sauerbrey equation using the Qtools software provided by Biolin Scientitic.

3. Results and discussion

We prepared uTFC membranes by performing the interfacial polymerization of low-concentration TMC and MPD on a PVC substrate (Figure 1). In order to achieve improved membrane selectivity, amphiphilic copolymers of PMcH was blended into PVC for the preparation of a reactable PVC substrate (PVC-r) via non-solvent induced phase separation method [23, 25]. The hydroxyl groups (-OH) contained in PMcH is designed to react with TMC during the interfacial polymerization so that the polyamide rejection layer of the resulting ultrathin membrane (uTFC-r) is reinforced by the PMcH polymer chains. For comparison purpose, ultrathin membranes (uTFC-0) were also prepared on a control PVC substrate containing no PMcH (PVC-0).

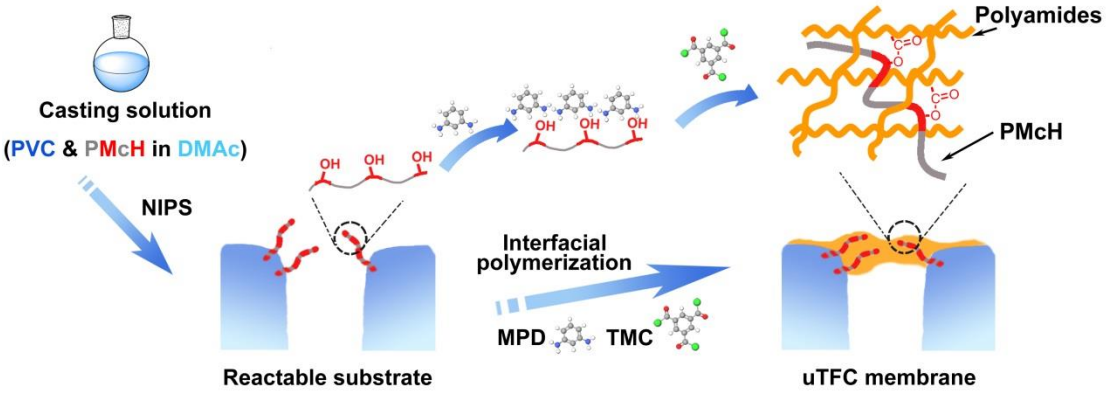

Figure 1 Schematic of the preparation process for uTFC-r membranes by interfacial

polymerization on a substrate containing reactable PMcH polymer chains.

3.1. Characterization of uTFC membranes

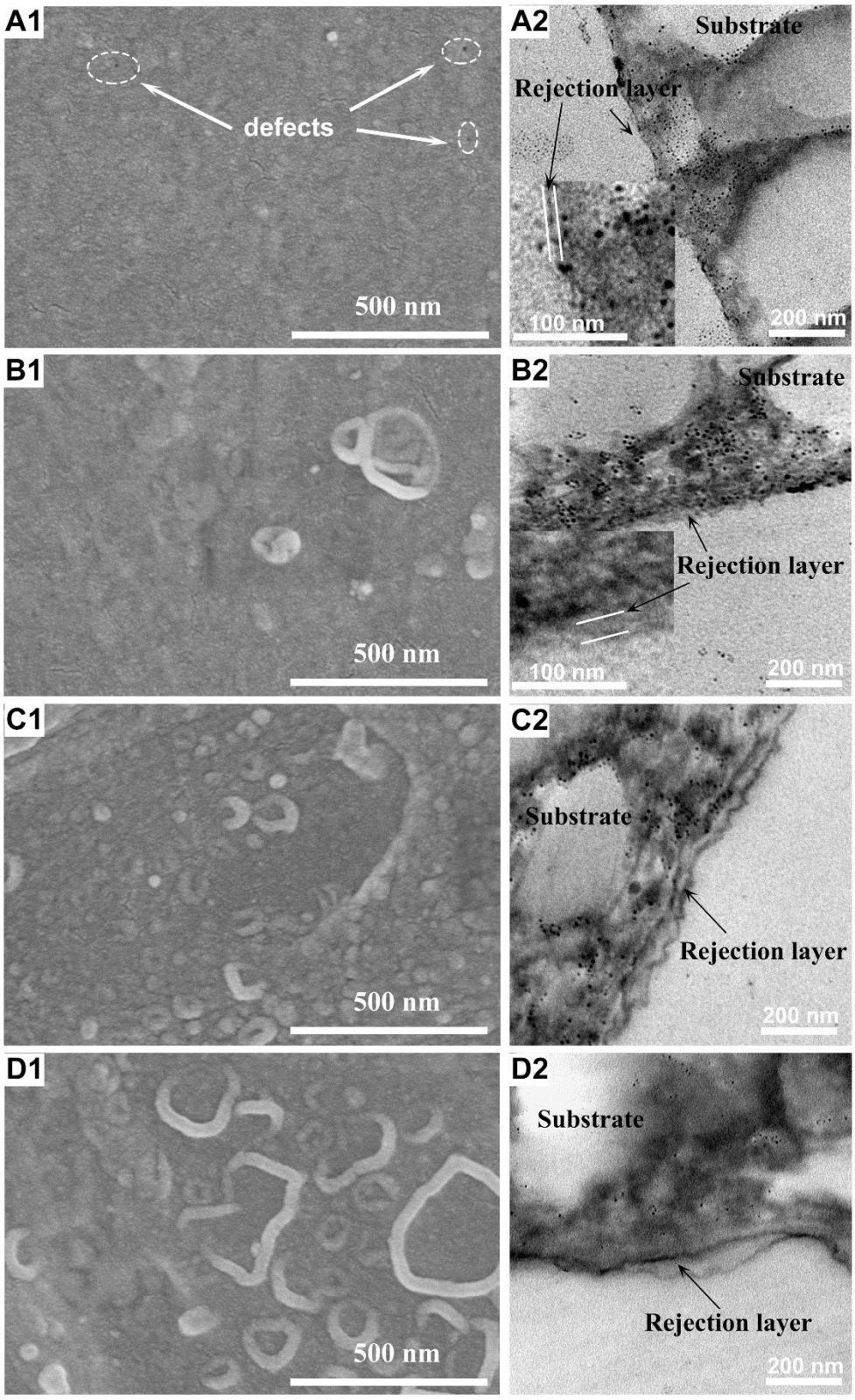

Figure 2 Morphologies of uTFC membranes: (A) uTFC-0-0.01; (B) uTFC-r-0.01; (C)

uTFC-r-0.02 and (D) uTFC-r-0.05. Panel 1 on the left shows the SEM micrographs of the membrane surfaces and Panel 2 on the right shows the TEM micrographs of the membrane cross-sections.

Membrane morphologies of the uTFC membranes with or without reinforcement by PMcH polymer chains were characterized by scanning electron microscopy (SEM, Figure 2 left panel) and transmission electron microscopy (TEM, Figure 2 right panel). The membrane uTFC-0-0.01 formed on the control substrate PVC-0 had a smooth surface (Figure 2A1), and its rejection layer thickness was on the order of 10 nm (Figure 2A2). This ultrathin rejection layer had numerous defects (see the pinholes in Figure 2A1). In comparison, the membrane uTFC-r-0.01 prepared on the reactable substrate PVC-r under otherwise identical synthesis conditions had a thicker rejection layer of approximately 20 nm with no observable pinholes (Figure 2B1). The thicker rejection layer formed on the reactable substrate can be attributed to the strong affinity of MPD to PMcH polymers contained in PVC-r. Quartz crystal microbalance results show much higher sorption of MPD by PMcH compared to PVC (Figure 3), possibly as a result of the polar functional groups (e.g., -OH) present in PMcH and their ability to form hydrogen bonding with MPD [18, 23, 26, 27].

For the polymer reinforced uTFC-r membranes, increasing MPD concentration from 0.01 to 0.05 wt% significantly increased the thickness of the resulting polyamide

rejection layer (Figure 2B-D). Meanwhile, the membrane surface became rougher due to the increased presence of nodular roughness features. These features are characteristic to polyamide membranes formed by the interfacial polymerization between MPD and TMC. According to the literature [28, 29], the surface roughness of polyamide membranes increases at higher monomer concentration. Some recent studies [7, 30, 31] further reveal that these nodular roughness structures are formed due to the degassing of CO_2 nanobubbles as a result of heat and acid generation during the interfacial polymerization. Higher monomer concentrations lead to greater amount of heat and H^+ generation and therefore rougher polyamide membrane surfaces.

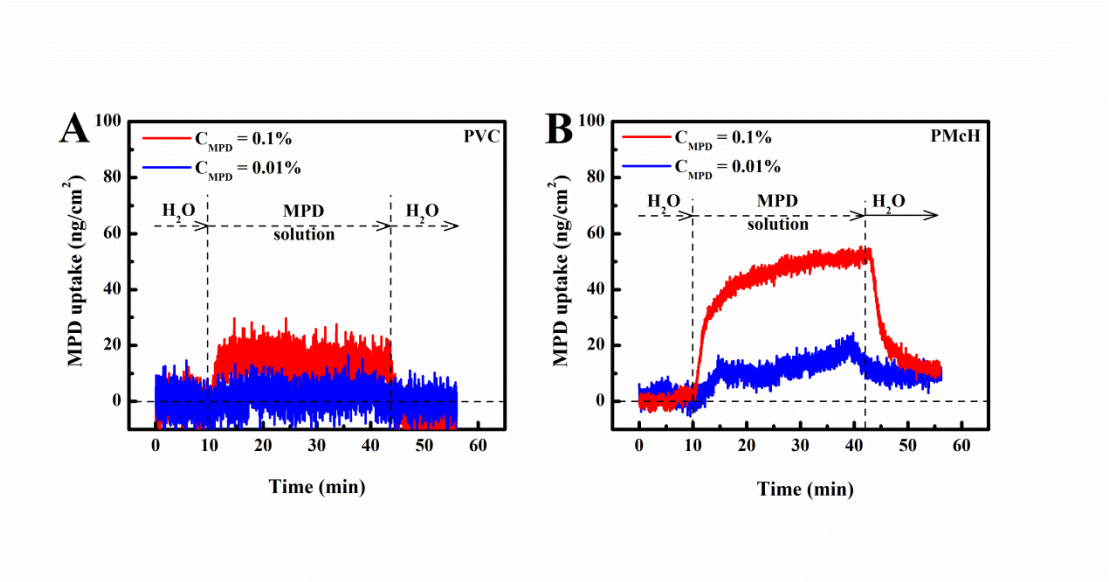

Figure 3 Sorption of MPD by (A) PVC and (B) PMcH. In a typical test, a thin PVC or PMcH layer was coated onto the Au resonator. The coater resonator was first exposed to deionized water for 10 min and then exposed to an MPD solution (0.1 wt%

or 0.01 wt%) to initiate the sorption measurement. After a 30-min sorption, the MPD-sorbed resonator was subject to a 10-min desorption using deionized water.

Surface chemical compositions of the uTFC membranes were evaluated on the basis of XPS results (Figure 4, Table S2, Table S3, and Table S4). Compared to uTFC-0-0.01, the reinforced membrane uTFC-r-0.01 had a much weaker Cl 2p peak (17.3 ± 0.5 % vs. 2.1 ± 0.3 %), which is consistent with its thicker polyamide rejection layer that would mask the Cl signals from the PVC substrate. This Cl 2p became barely detectable with the thicker polyamide layers formed at greater MPD concentration (0.02 - 0.1 wt%). Compared with uTFC-0-0.01, the reinforced membrane uTFC-r-0.01 had a much stronger N 1s peak (Figure 4A and Table S2). It demonstrated that more polyamides should be formed on the substrate of PVC-r. This result can also be explained by the strong affinity of MPD to PMcH polymers contained in PVC-r. This N 1s peak became stronger with the thicker polyamide layers formation.

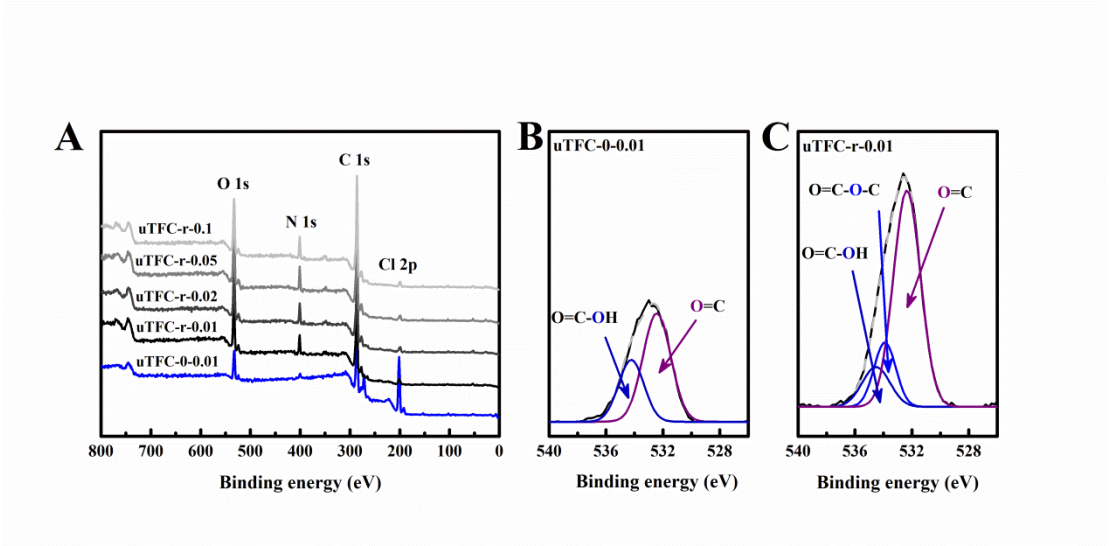

Figure 4 XPS spectra of prepared uTFC membranes (A), high resolution XPS spectra of O 1s foruTFC-0-0.01 (B) and uTFC-r-0.01 (C). The binding energy shifts of **O**=C (including **O**=C-O-H, **O**=C-O-C and **O**=C-N-C), O=C-**O**-C and O=C- **O**-H were 532.3 ±0.1 eV, 533.9 ±0.1 eV and 534.5 ±0.3 eV, respectively.

To better understand the surface chemical compositions of the uTFC membranes, the high resolution O1s peak was deconvolved to carbonyl group (**O**=C, including **O**=C-O-H, **O**=C-O-C and **O**=C-N-C, 532.3 ±0.1 eV), ester group (**O**=C-O-C, 533.9 ±0.1 eV) and carboxyl group (O=C-**O**-H, 534.5 ±0.3 eV) [32-34]. Based on the deconvolution, the content of carbonyl group, ester group, carboxyl group and amide group (O=C-N-C) were calculated (Table S2). Our analysis revealed a higher amide group content in the reinforced membrane uTFC-r-0.01 compared with uTFC-0-0.01 (Table S2), which is consistent with its stronger N peak in Figure 4A. Moreover, the signals attributed to ester groups were only observed in the uTFC-r membranes (Figure 4B, 4C), which can be explained by the reaction between the acyl chloride

groups (O=C-Cl) of TMC and the hydroxyl groups (-OH) in the reactable substrate [23, 35, 36]. This result revealed the additional role of the reactable copolymers in participating in the interfacial polymerization. The formation of ester groups, together with higher adsorbed MPD concentration, resulted in a thicker and reinforced rejection layer.

By adjusting the incident angle in XPS tests, the surface composition of the uTFC membranes in different depth can be collected [37]. The N content (amide group content) of uTFC-r-0.01 increased with the increasing of inspection depth (Table S3, Table S4). In contrast, the N content of uTFC-0-0.01 increased first (when inspection depth increased from 5 to 8.7 nm) and then decreased (when inspection depth further increased to 10 nm, Table S3). Since no N 1s signals were observed in PVC-0 and PVC-r (Figure S1A), these N content variations revealed that the rejection layer of uTFC-0-0.01 was really thicker than the one of uTFC-r-0.01 and its thickness was in the range of 10 nm. The content of carboxyl group of both the uTFC-r-0.01 and uTFC-0-0.01 decreased with the increasing of inspection depth (Table S4). It implied that more carboxyl groups were formed in the organic side (n-hexane solution) due to the excessive TMC [21, 38, 39]. At the smallest inspection depth of 5 nm, uTFC-r-0.01 had slightly higher carboxyl content than uTFC-0-0.01 (3.7 ± 0.2 % vs. 3.3 ± 0.1 %), which explains the more negative zeta potential of the former (Figure 5A). The more negatively charged membrane surface would benefit the rejection of

divalent anions (e.g. SO_4^{2-}) by the uTFC-r-0.01 as a result of enhanced Donnan exclusion [36, 40].

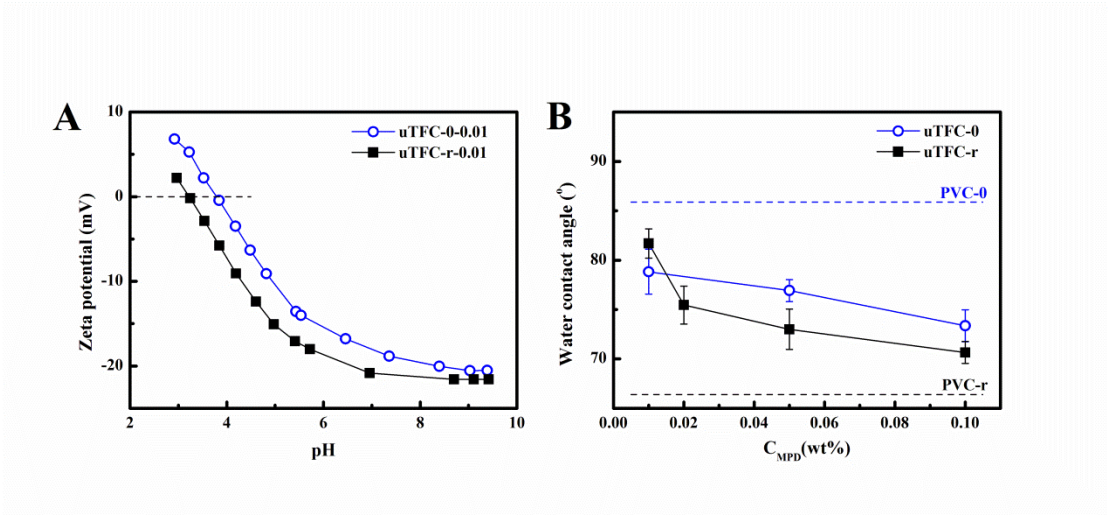

Figure 5 Zeta-potential curves of uTFC-0-0.01 and uTFC-r-0.01 (A) and water contact angle of the prepared uTFC membranes (B).

The prepared uTFC-r membranes all showed negatively charged surfaces (Figure 5A and S3). With the increasing of C_{MPD}, surface charge of uTFC-r membranes reduced slightly (Figure S3), implied a higher crosslinked rejection layer of the uTFC-r membrane with higher C_{MPD} [38, 41]. Compared with uTFC-0-0.01, the water contact angles of uTFC-r-0.01 were slightly higher (Figure 5B), which can be explained by the formation of additional polyester groups in uTFC-r-0.01 that are less hydrophilic compared to polyamide groups [18, 42]. Except for the low C_{MPD} condition, the water contact angles of the uTFC membranes were much lower than the ones of uTFC-0

membranes, due to their higher hydrophilic polyamide group contents (Table S2). The negatively charged surface properties and the variation on surface hydropilicities were consistent with the XPS results of the formation of amide groups, ester groups and carboxyl groups in rejection layer.

3.2. Performance of the uTFC membranes

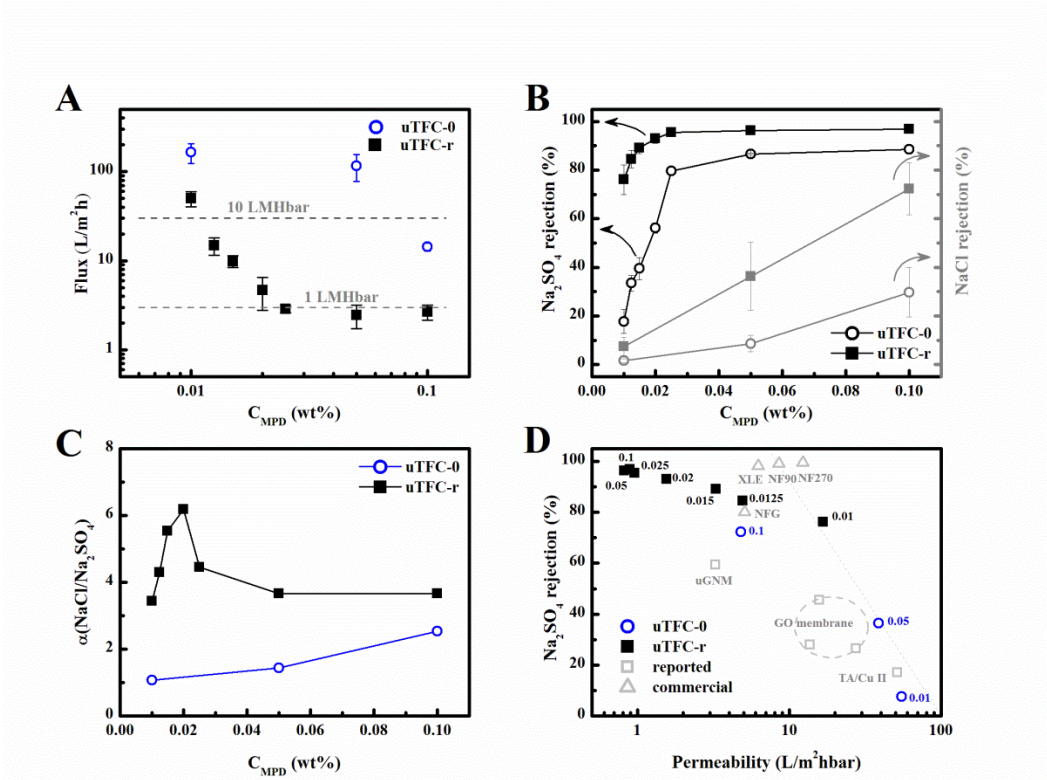

Figure 6 Performance of the prepared uTFC membranes: (A) Water flux, (B) Na_2SO_4 (black) and NaCl (gray) rejections, (C) Na_2SO_4 to NaCl selectivities ($\alpha(NaCl/Na_2SO_4)$) and (D) Na_2SO_4 rejection versus water permeabilities of uTFC membranes prepared in this work, ultrathin graphene nanofiltration membrane (uGNM) [43], graphene oxide (GO) membranes [44], bio-polyphenols and transitional metals networks coated

membrane (TA/Cu II) [45], commercial TFC membranes: NF270, NF90, XLE (tested in this work and received from Dow FilmTec) and NFG (tested in this work and received from Synder Filtration, Inc.).

The performance includes pure water flux, Na_2SO_4 rejection (R_{Na2SO4}), NaCl rejection (R_{NaCl}) and Na_2SO_4 to NaCl selectivity ($\alpha(NaCl/Na_2SO_4)$) of the uTFC membranes are presented in Figure 6A, B and C. Compared to the uTFC-0-0.01, the polymer reinforced membrane uTFC-r-0.01 showed lower water flux but much higher salts rejection and greatly improved Na_2SO_4 to NaCl selectivity. This result can be explained by the formation of no observable pinholes contained (SEM in Figure 2) and much denser (XPS results in Figure 4 and Table S2) ultrathin polyamide rejection layer reinforced by the polymer chains in the reactable substrate (PVC-r).

The influence of C_{MPD} in interfacial polymerization process on the performance of the uTFC membrane was also investigated. For the control uTFC-0 membranes, with the increasing of C_{MPD}, the water flux greatly reduced, the salts rejection significantly increased and the Na_2SO_4 to NaCl selectivity slightly increased. For the reinforced uTFC-r membranes, when C_{MPD} increased from 0.01 wt% to 0.02 wt%, the water flux greatly reduced, while R_{Na2SO4}, R_{NaCl} and $\alpha(NaCl/Na_2SO_4)$ greatly increased. However, further increased the C_{MPD}, the water flux and salts rejection changed slightly (the flux

were around 3 L/(m^2 h), R_{Na2SO4} > 90% and R_{NaCl} > 80%), α($NaCl/Na_2SO_4$) even reduced (from 4.44 to 3.66). The formation of an ultrathin rejection layer due to the low C_{MPD} in interfacial polymerization process was supposed to be the main reason for these performance variations [5, 13]. As mentioned in section 3.1, with the decreasing of C_{MPD}, the rejection layer became thinner and looser (SEM in Figure 2, XPS results in Table S2, S3), which commonly resulted to the increase of water flux, greatly decreasing of R_{NaCl} [13-15]. Compared with uTFC-0, the much higher R_{Na2SO4} of the uTFC-r membranes can be explained by the higher crosslink degree of the rejection layer due to the reinforcement by polymer chains (XPS results in Table S2, S3) and partly the Donnan exclusion due to the negatively charged surface properties [36, 40].

The divalent salts rejection efficiency of the uTFC membranes were evaluated and displayed in Figure 6D. In comparison, the corresponding results of some commercial TFC membranes and reported membranes with ultrathin rejection layers were also calculated. Most of the prepared uTFC membranes with relatively high C_{MPD} showed high Na_2SO_4 rejection (R_{Na2SO4} > 90%) but low water permeability (< 5 L/(m^2 h bar)). The uTFC-0-0.01, uTFC-0-0.05 and some of the reported membranes with advanced functional materials (GO, tannic acid-copper complexes) constructed ultrathin rejection layer [43-45] exhibited much higher water permeability (> 10 L/(m^2 h bar)), but lower Na_2SO_4 rejection (< 50%). Some of the commercial TFC membranes

(NF270, NF90 and XLE) showed high divalent salts rejection efficiency. The commercial NF270 membrane even showed both high Na_2SO_4 rejection (R_{Na2SO4} > 95%) and high water permeability (> 12 L/(m^2 h bar)). Considering the trade-off relationship [45], the reinforced membrane uTFC-r-0.01 also showed comparable divalent salts rejection efficiency with the highly optimized commercial TFC membranes. Its water permeability (16.7 ± 3.2 L/(m^2 h bar)) was even about 3 times higher than the commercial NFG membrane (5.1 ± 1.4 L/(m^2 h bar)). These separation properties of the reinforced uTFC membranes showed the application potential in desalination pretreatment and water softening with high efficiency [39, 47-50].

4. Conclusion

uTFC membranes with polymer chains reinforced ultrathin rejection layer were designed and prepared based on reactable polymer chains contained substrates (PVC-r) by interfacial polymerization using MPD with very low concentrations as aqueous phase and TMC solution as organic phase. The resulting uTFC-r-0.01 membrane showed high water permeability, and greatly improved Na_2SO_4 to NaCl selectivity. Our study revealed that the esterification between TMC and PMcH and the great adsorption of MPD by PMcH chains were the main reasons for the formation of the dense and ultrathin layer. These findings have important implications for providing a facile way to design and construct uniform ultrathin layers as well as to prepare TFC membranes with ultrathin rejection layers by interfacial polymerization. The prepared

uTFC membranes exhibited the potential application in desalination pretreatment and water softening with high efficiency.

Supporting Information

Supporting Information includes the characterization for PVC-0 (XPS), PVC-r (XPS) and uTFC membranes (SEM, XPS and zeta potential).

Acknowledgments

We acknowledge the support from the General Research Fund (17207514) by the Research Grants Council of Hong Kong, the Strategic Research Theme (Clean Energy) and the Seed Grant for Basic Research (201511159141) of the University of Hong Kong. We appreciate the partial support from the 111 Talent Program, the Programme of Introducing Talents of Discipline to Universities (B13012) and the Haitian Scholar Program from Dalian University of Technology. We also thank Prof. Baoku Zhu, Mr. Mingyong Zhou and Dr. Chuner Lin for the help on amphiphilic copolymer characterization.

References

[1] D. Li, H. Wang, Recent developments in reverse osmosis desalination membranes, Journal of Materials Chemistry, 20 (2010) 4551.

[2] M. Elimelech, W.A. Phillip, The future of seawater desalination: energy,

technology, and the environment, Science, 333 (2011) 712-717.

[3] W.J. Lau, A.F. Ismail, N. Misdan, M.A. Kassim, A recent progress in thin film composite membrane: A review, Desalination, 287 (2012) 190-199.

[4] S. Kim, K.H. Chu, Y.A.J. Al-Hamadani, C.M. Park, M. Jang, D.-H. Kim, M. Yu, J. Heo, Y. Yoon, Removal of contaminants of emerging concern by membranes in water and wastewater: A review, Chemical Engineering Journal, 335 (2018) 896-914.

[5] A.K. Ghosh, B.-H. Jeong, X. Huang, E.M.V. Hoek, Impacts of reaction and curing conditions on polyamide composite reverse osmosis membrane properties, Journal of Membrane Science, 311 (2008) 34-45.

[6] P. Gorgojo, S. Karan, H.C. Wong, M.F. Jimenez-Solomon, J.T. Cabral, A.G. Livingston, Ultrathin polymer films with intrinsic microporosity: Anomalous solvent permeation and high flux membranes, Advanced Functional Materials, 24 (2014) 4729-4737.

[7] X.-H. Ma, Z.-K. Yao, Z. Yang, H. Guo, Z.-L. Xu, C.Y. Tang, M. Elimelech, Nanofoaming of polyamide desalination membranes to tune permeability and selectivity, Environmental Science & Technology Letters, 5 (2018) 123-130.

[8] Z. Tan, S. Chen, X. Peng, L. Zhang, C. Gao, Polyamide membranes with nanoscale Turing structures for water purification, Science, 360 (2018) 518-521.

[9] M. Shi, Z. Wang, S. Zhao, J. Wang, P. Zhang, X. Cao, A novel pathway for high performance RO membrane: Preparing active layer with decreased thickness and enhanced compactness by incorporating tannic acid into the support, Journal of

Membrane Science, 555 (2018) 157-168.

[10] D.L. Gin, R.D. Noble, Designing the next generation of chemical separation membranes, Science, 332 (2011) 674-676.

[11] D.L. Oatley-Radcliffe, M. Walters, T.J. Ainscough, P.M. Williams, A.W. Mohammad, N. Hilal, Nanofiltration membranes and processes: A review of research trends over the past decade, Journal of Water Process Engineering, 19 (2017) 164-171.

[12] J. Wang, L. Qin, J. Lin, J. Zhu, Y. Zhang, J. Liu, B. Van der Bruggen, Enzymatic construction of antibacterial ultrathin membranes for dyes removal, Chemical Engineering Journal, 323 (2017) 56-63.

[13] A.P. Rao, S.V. Joshi, J.J. Trivedi, C.V. Devmurari, V.J. Shah, Structure–performance correlation of polyamide thin film composite membranes effect of coating conditions on film formation, Journal of Membrane Science, 211 (2003) 13-24.

[14] R.R. Nair, H.A. Wu, P.N. Jayaram, I.V. Grigorieva, A.K. Geim, Unimpeded permeation of water through helium-leak–tight graphene-based membranes, Science, 335 (2012) 442-444.

[15] Y. Zhu, W. Xie, S. Gao, F. Zhang, W. Zhang, Z. Liu, J. Jin, Single-walled carbon nanotube film supported nanofiltration membrane with a nearly 10 nm thick polyamide selective layer for high-flux and high-rejection desalination, Small, 12 (2016) 5034-5041.

[16] X.-H. Ma, Z. Yang, Z.-K. Yao, H. Guo, Z.-L. Xu, C.Y. Tang, Interfacial polymerization with electrosprayed microdroplets: Toward controllable and ultrathin polyamide membranes, Environmental Science & Technology Letters, 5 (2018) 117-122.

[17] S. Karan, Z. Jiang, A.G. Livingston, Sub-10 nm polyamide nanofilms with ultrafast solvent transport for molecular separation, Science, 348 (2015) 1347-1351.

[18] A.K. Ghosh, E.M.V. Hoek, Impacts of support membrane structure and chemistry on polyamide–polysulfone interfacial composite membranes, Journal of Membrane Science, 336 (2009) 140-148.

[19] L. Wang, M. Fang, J. Liu, J. He, J. Li, J. Lei, Layer-by-layer fabrication of high-performance polyamide/ZIF-8 nanocomposite membrane for nanofiltration applications, ACS Applied Materials & Interfaces, 7 (2015) 24082-24093.

[20] Z. Yang, Z.W. Zhou, H. Guo, Z. Yao, X.H. Ma, X. Song, S.P. Feng, C.Y. Tang, Tannic acid/$Fe3^{+}$ nanoscaffold for interfacial polymerization: Toward enhanced nanofiltration performance, Environmental Science & Technology, 52 (2018) 9341-9349.

[21] J.E. Gu, S. Lee, C.M. Stafford, J.S. Lee, W. Choi, B.Y. Kim, K.Y. Baek, E.P. Chan, J.Y. Chung, J. Bang, J.H. Lee, Molecular layer-by-layer assembled thin-film composite membranes for water desalination, Advanced Materials, 25 (2013) 4778-4782.

[22] X. Song, S. Qi, C.Y. Tang, C. Gao, Ultra-thin, multi-layered polyamide

membranes: Synthesis and characterization, Journal of Membrane Science, 540 (2017) 10-18.

[23] Z. Yao, H. Guo, Z. Yang, C. Lin, B. Zhu, Y. Dong, C.Y. Tang, Reactable substrate participating interfacial polymerization for thin film composite membranes with enhanced salt rejection performance, Desalination, 436 (2018) 1-7.

[24] Z. Yao, S. Du, Y. Zhang, B. Zhu, L. Zhu, A.E. John, Positively charged membrane for removing low concentration Cr(VI) in ultrafiltration process, Journal of Water Process Engineering, 8 (2015) 99-107.

[25] Z. Yao, Y. Li, Y. Cui, K. Zheng, B. Zhu, H. Xu, L. Zhu, Tertiary amine block copolymer containing ultrafiltration membrane with pH-dependent macromolecule sieving and Cr(VI) removal properties, Desalination, 355 (2015) 91-98.

[26] X. Li, K.Y. Wang, B. Helmer, T.-S. Chung, Thin-film composite membranes and formation mechanism of thin-film layers on hydrophilic cellulose acetate propionate substrates for forward osmosis processes, Industrial & Engineering Chemistry Research, 51 (2012) 10039-10050.

[27] B. Liu, C. Chen, P. Zhao, T. Li, C. Liu, Q. Wang, Y. Chen, J. Crittenden, Thin-film composite forward osmosis membranes with substrate layer composed of polysulfone blended with PEG or polysulfone grafted PEG methyl ether methacrylate, Frontiers of Chemical Science and Engineering, 10 (2016) 562-574.

[28] H.I. Kim, S.S. Kim, Plasma treatment of polypropylene and polysulfone supports for thin film composite reverse osmosis membrane, Journal of Membrane Science,

286 (2006) 193-201.

[29] B. Khorshidi, T. Thundat, B.A. Fleck, M. Sadrzadeh, A novel approach toward fabrication of high performance thin film composite polyamide membranes, Scientific Reports, 6 (2016) 22069.

[30] X. Ma, Z. Yang, Z. Yao, H. Guo, Z. Xu, C.Y. Tang, Tuning roughness features of thin film composite polyamide membranes for simultaneously enhanced permeability, selectivity and anti-fouling performance, Journal of colloid and interface science, 540 (2019) 382-388.

[31] X. Song, B. Gan, Z. Yang, C.Y. Tang, C. Gao, Confined nanobubbles shape the surface roughness structures of thin film composite polyamide desalination membranes, Journal of Membrane Science, 582 (2019) 342-349.

[32] G.P. López, D.G. Castner, B.D. Ratner, XPS O 1s binding energies for polymers containing hydroxyl, ether, ketone and ester groups, Surface and Interface Analysis, 17 (1991) 267-272.

[33] U.Zielke, K.J.Hüttinger, W.P.Hoffman, Surface-oxidized carbon fibers: I. Surface structure and chemistry, Carbon, 34 (1996) 983-998.

[34] J.-H. Zhou, Z.-J. Sui, J. Zhu, P. Li, D. Chen, Y.-C. Dai, W.-K. Yuan, Characterization of surface oxygen complexes on carbon nanofibers by TPD, XPS and FT-IR, Carbon, 45 (2007) 785-796.

[35] L.F. Villalobos, T. Huang, K.V. Peinemann, Cyclodextrin Films with Fast Solvent Transport and Shape-Selective Permeability, Advanced Materials, 29 (2017) 1606641.

[36] Z. Yao, H. Guo, Z. Yang, W. Qing, C.Y. Tang, Preparation of nanocavity-contained thin film composite nanofiltration membranes with enhanced permeability and divalent to monovalent ion selectivity, Desalination, 445 (2018) 115-122.

[37] Y. Cui, Z.-K. Yao, K. Zheng, S.-Y. Du, B.-K. Zhu, L.-P. Zhu, C.-H. Du, Positively-charged nanofiltration membrane formed by quaternization and cross-linking of blend PVC/P(DMA-co-MMA) precursors, Journal of Membrane Science, 492 (2015) 187-196.

[38] C. Tang, Y. Kwon, J. Leckie, Probing the nano- and micro-scales of reverse osmosis membranes—A comprehensive characterization of physiochemical properties of uncoated and coated membranes by XPS, TEM, ATR-FTIR, and streaming potential measurements, Journal of Membrane Science, 287 (2007) 146-156.

[39] A.G. Fane, R. Wang, M.X. Hu, Synthetic membranes for water purification: status and future, Angewandte Chemie International Edition, 54 (2015) 3368-3386.

[40] M. Paul, S.D. Jons, Chemistry and fabrication of polymeric nanofiltration membranes: A review, Polymer, 103 (2016) 417-456.

[41] V.T. Do, C.Y. Tang, M. Reinhard, J.O. Leckie, Degradation of polyamide nanofiltration and reverse osmosis membranes by hypochlorite, Environmental Science & Technology, 46 (2012) 852-859.

[42] H. Dave, L. Ledwani, N. Chandwani, P. Kikani, B. Desai, M.B. Chowdhuri, S.K. Nema, Use of dielectric barrier discharge in air for surface modification of polyester

substrate to confer durable wettability and enhance dye uptake with natural dye eco-alizarin, Composite Interfaces, 19 (2012) 219-229.

[43] Y. Han, Z. Xu, C. Gao, Ultrathin Graphene Nanofiltration Membrane for Water Purification, Advanced Functional Materials, 23 (2013) 3693-3700.

[44] M. Hu, B. Mi, Enabling graphene oxide nanosheets as water separation membranes, Environmental Science & Technology, 47 (2013) 3715-3723.

[45] T. Chakrabarty, L. Pérez-Manríquez, P. Neelakanda, K.-V. Peinemann, Bioinspired tannic acid-copper complexes as selective coating for nanofiltration membranes, Separation and Purification Technology, 184 (2017) 188-194.

[46] G.M. Geise, H.B. Park, A.C. Sagle, B.D. Freeman, J.E. McGrath, Water permeability and water/salt selectivity tradeoff in polymers for desalination, Journal of Membrane Science, 369 (2011) 130-138.

[47] S. Jamaly, N.N. Darwish, I. Ahmed, S.W. Hasan, A short review on reverse osmosis pretreatment technologies, Desalination, 354 (2014) 30-38.

[48] D. Zhou, L. Zhu, Y. Fu, M. Zhu, L. Xue, Development of lower cost seawater desalination processes using nanofiltration technologies — A review, Desalination, 376 (2015) 109-116.

[49] O.A. Hamed, Overview of hybrid desalination systems — current status and future prospects, Desalination, 186 (2005) 207-214.

[50] L. Henthorne, B. Boysen, State-of-the-art of reverse osmosis desalination pretreatment, Desalination, 356 (2015) 129-139.

Supporting Information

Highly permeable and highly selective ultrathin film composite polyamide membranes reinforced by reactable polymer chains

Zhikan Yao[a], Zhe Yang[a], Hao Guo[a], Xiaohua Ma[a,b], Yingchao Dong[c], and Chuyang Y. Tang[a*]

a. Department of Civil Engineering, The University of Hong Kong, Pokfulam, Hong Kong SAR.

b. Shanghai Key Laboratory of Multiphase Materials Chemical Engineering, Chemical Engineering Research Center, East China University of Science and Technology, 130 Meilong Road, Shanghai, China

c. Key Laboratory of Industrial Ecology and Environmental Engineering (MOE), School of Environmental Science and Technology, Dalian University of Technology, Dalian, China

*Corresponding author.

E-mail address: tangc@hku.hk (C.Y. Tang)

S1 Characterization of substrates

Surface chemical compositions of the prepared substrates were characterized and listed in Table S1 and Figure S1. A strong O 1s peak was observed in the XPS spectrum of PVC-r, due to the existence of PMcH in the substrate surface [1]. For the sake of a better understanding of the surface chemical compositions of PVC-r, AugerScan 3.2 software was employed to deconvolve the high resolution O1s peak. The O 1s peak was splited into O-C=O (532.3 eV), O-C=O (533.9 eV) and C-O-H (533.1 eV) [2, 3].

Table S1 The surface compositions of substrates.

ID	C 1s (%)[1]	O 1s				Cl 2p (%)[1]
		O=C (%)	O=C-**O** (%)	C-**O**-H (%)	Total (%)	
PVC-0	70.3	-	-	-	-	29.7
PVC-r	69.2	7.3	7.2	5.2	19.7	11.1

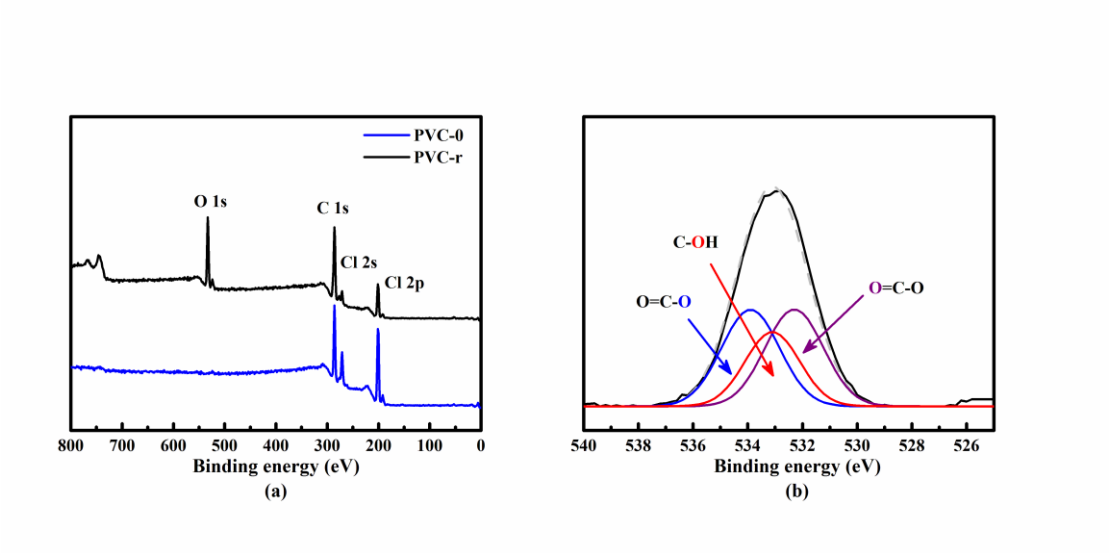

Figure S1 XPS results: (a) XPS spectra of PVC-0 and PVC-r, (b) O 1s high resolution XPS spectra of PVC-r. The binding energy shift of **O**=C, **O**=C-O-C and C-**O**-H were

532.3 eV, 533.9 eV and 533.1 eV, respectively [2, 3]. The inspection depth is about 8.7 nm.

S2 Characterization of uTFC membranes

Figure S2 shows the cross-section SEM images of uTFC-0-0.01, uTFC-r-0.01, uTFC-r-0.02, uTFC-r-0.05, uTFC-r-0.1 and the surface SEM images of uTFC-r-0.1.

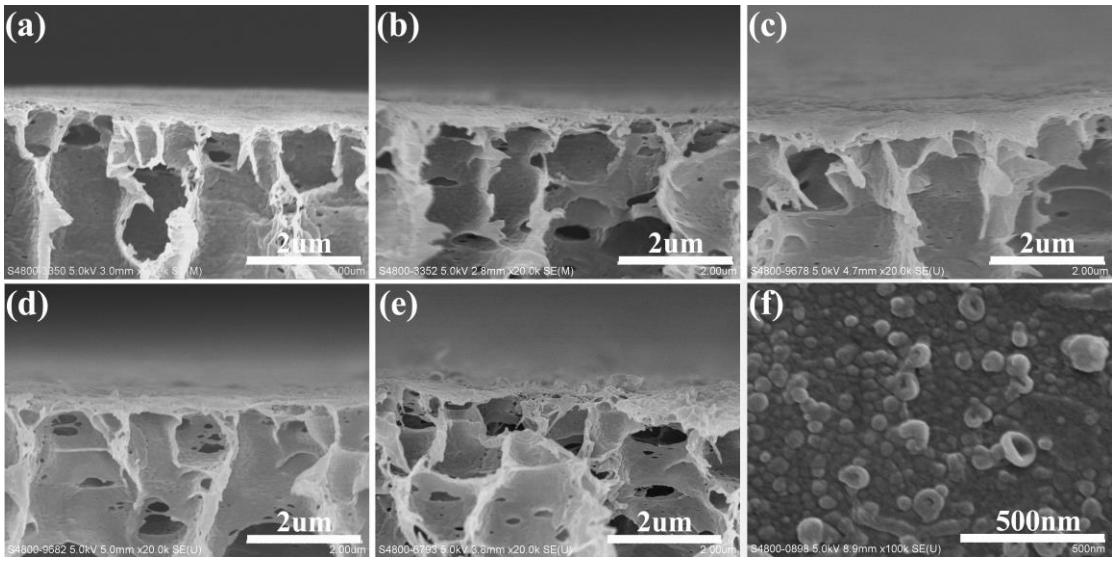

Figure S2 Cross-section SEM images of (a) uTFC-0-0.01, (b) uTFC-r-0.01, (c) uTFC-r-0.02, (d) uTFC-r-0.05 (e) uTFC-r-0.1 and surface SEM image of (f) uTFC-r-0.1.

Table S2 The surface chemical compositions of prepared uTFC membranes[a].

ID	uTFC-0-0.01	uTFC-r-0.01	uTFC-r-0.02	uTFC-r-0.05	uTFC-r-0.1
C 1s (%)	71.3 ±0.2	76.0 ±0.2	75.8	76.1	76.0
O 1s (%)	8.7 ±0.3	15.6 ±0.3	15.0	14.9	14.6
N 1s (%)	2.7 ±0.1	6.3 ±0.1	7.1	7.2	7.7
Cl 2p (%)	17.3 ±0.5	2.1 ±0.3	2.1	1.8	1.7
O=C-OH[b] (%)	3.0 ±0.1	2.1 ±0.1	2.0	1.9	1.7

O=C-O-C[b] (%)	-	2.6 ±0.1	2.0	1.9	1.8
O=C-N-C[b] (%)	2.8 ±0.1	6.3 ±0.1	7.1	7.2	7.7

a. The inspection depth is about 8.7 nm.

b. The content of O=C-OH, O=C-O-C and O=C-N-C were calculated according to the O 1s high resolution XPS spectra.

Table S3 The surface chemical compositions of uTFC-0-0.01 and uTFC-r-0.01 with different inspection depth.

Inspection depth (nm)	uTFC-0-0.01				uTFC-r-0.01			
	C 1s (%)	O 1s (%)	N 1s (%)	Cl 2p (%)	C 1s (%)	O 1s (%)	N 1s (%)	Cl 2p (%)
5.0	71.7 ± 0.5	8.9 ± 0.1	2.3 ± 0.1	17.1 ± 0.5	77.8 ± 0.5	15.5 ± 0.5	5.4 ± 0.1	1.3 ± 0.1
8.7	71.3 ± 0.2	8.7 ± 0.3	2.7 ± 0.1	17.3 ± 0.5	76.0 ± 0.2	15.6 ± 0.3	6.3 ± 0.1	2.1 ± 0.3
10.0	72.2 ± 0.3	7.8 ± 0.4	2.1 ± 0.1	17.9 ± 0.3	74.5 ± 0.1	16.2 ± 0.3	6.9 ± 0.1	2.4 ± 0.3

Table S4 The functional groups content in the surface of uTFC-0-0.01 and uTFC-r-0.01 with different inspection depth.

Inspection depth (nm)	uTFC-0-0.01			uTFC-r-0.01		
	O=C-OH (%)	O=C-O-C (%)	O=C-N-C (%)	O=C-OH (%)	O=C-O-C (%)	O=C-N-C (%)
5.0	3.3 ±0.1	-	2.3 ±0.1	3.7 ±0.2	1.3 ±0.1	5.5 ±0.2
8.7	3.0 ±0.1	-	2.8 ±0.1	2.1 ±0.1	2.6 ±0.1	6.3 ±0.1
10.0	2.8 ±0.1	-	2.2 ±0.1	1.7 ±0.1	3.0 ±0.2	6.9 ±0.2

Table S2, Table S3 and Table S4 shows the surface chemical compositions of prepared uTFC membranes based on XPS measurements. It can be found from Table S2 that,

the amide group content increased and the carboxyl group content decreased with the thicker polyamide layers formation (the increasing of C_{MPD}). It revealed that with the increasing of C_{MPD}, the crosslink degree of polyamides increased and the rejection layer became denser.

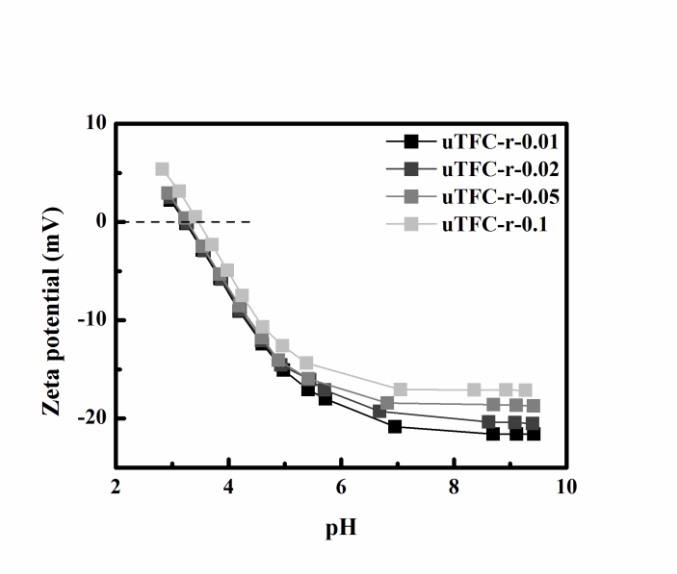

Figure S3 Zeta-potential curves of uTFC-r membranes.

Figure S3 shows the zeta-potential curves of uTFC-r membranes with different C_{MPD}.

Reference

[1] Z. Yao, H. Guo, Z. Yang, C. Lin, B. Zhu, Y. Dong, C.Y. Tang, Reactable substrate participating interfacial polymerization for thin film composite membranes with enhanced salt rejection performance, Desalination, 436 (2018) 1-7.

[2] Z.R. Yue, W. Jiang, L. Wang, S.D. Gardner, C.U. Pittman, Surface characterization of electrochemically oxidized carbon fibers, Carbon, 37 (1999) 1785-1796.

[3] J.-H. Zhou, Z.-J. Sui, J. Zhu, P. Li, D. Chen, Y.-C. Dai, W.-K. Yuan,

Characterization of surface oxygen complexes on carbon nanofibers by TPD, XPS and FT-IR, Carbon, 45 (2007) 785-796.